Supplementary information file

"Analysis of reduced paramagnetic shifts as an effective tool in NMR spectroscopy"

Alexander A. Pavlov, Valentin V. Novikov, Igor A. Nikovskiy, Elizaveta K. Melnikova, Yulia V. Nelyubina, Dmitry Y. Aleshin.

Table of Content

S.1. Derivation of the equations for the temperature dependence of both the contact and pseudocontact shifts within the spin-Hamiltonian approach.

Depending on the represented parameters, the following spin-Hamiltonians were used:

$$\hat{H} = D\left(\hat{S}_z^2 - \frac{1}{3}\hat{S}^2\right) + \mu_B B \cdot g \cdot \hat{S} + A_{iso}\hat{I} \cdot \hat{S},$$

$$\hat{H} = \sigma\lambda\hat{L} \cdot \hat{S} + \Delta\left(3\hat{L}_z^2 - \hat{L}^2\right) + \mu_B B(-\sigma\hat{L} + g\hat{S}) + A_{iso}\hat{I} \cdot \hat{S}.$$

(*D* – zero-field splitting energy; $\hat{S}$ and $\hat{L}$ – electronic spin and orbital operators, $\hat{S}_z$ and $\hat{L}_z$ – their projections; $\hat{I}$ – nuclear spin operator; *B* – external magnetic field of 14.1 T as observed in an NMR spectrometer with the proton Larmor frequency of 600 MHz; μ_B – Borh magneton; *g* – electronic g-tensor; A_{iso} – isotropic value of hyperfine interaction; λ – spin-orbit coupling; σ – orbital reduction factor; Δ – crystal field parameter).

The contact shift was calculated by the following equation:

$$\delta^{CS} = \frac{\sum \nu_i \cdot exp(-E_i/kT)}{\sum exp(-E_i/kT)} - \nu_0,$$

(ν_i – frequency of *i*-th Kramers doublet; E_i – energy of *i*-th Kramers doublet; ν_0 – Larmor frequency of a nucleus in the external magnetic field without any interactions with electrons (600 MHz)).

The pseudocontact shift was calculated by the following equation:

$$\delta^{pc} = \frac{1}{12\pi r^3}\Delta\chi_{ax}(3cos^2\theta - 1)$$

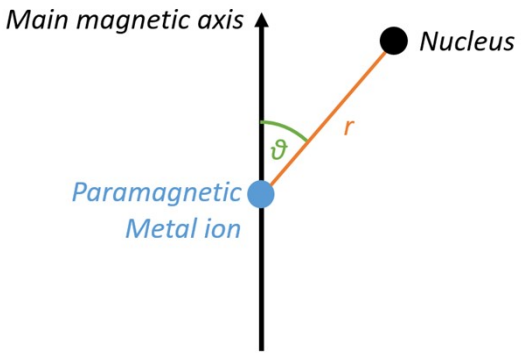

θ and *r* are polar coordinates of a nucleus relative to the main magnetic axis (see picture above).

For model calculations, $\theta = 0$ and $r = 10$ Å were used; $\Delta\chi_{ax}$ was calculated as follows:

$$\Delta\chi_{ax} = \chi_{zz} - \frac{\chi_{xx} + \chi_{yy}}{2}, \quad \chi_{aa} = \frac{N_A kT}{10} \frac{\partial^2}{\partial B_a^2} ln\left(\sum_i e^{-\frac{E_i}{kT}}\right),$$

(a – x, y, z; E_i – energy of i-th level).

Details are given below on how the temperature dependence of the contact and the pseudocontact shifts was described by the expressions 4 and 5 (see main text) in a typical temperature range from 200 to 400 K accessible in a common solution NMR experiment. Solid lines on the following plots are the fits by eq. 4b and 5b of the main text. Red and blue colors refer to the contact and the pseudocontact shifts, respectively.

S.1.1. Co(II), S = 3/2

A) $g_x = g_y = 2.30$, $g_z = 2.17$, $D = +12.7$ cm^{-1}.[1]

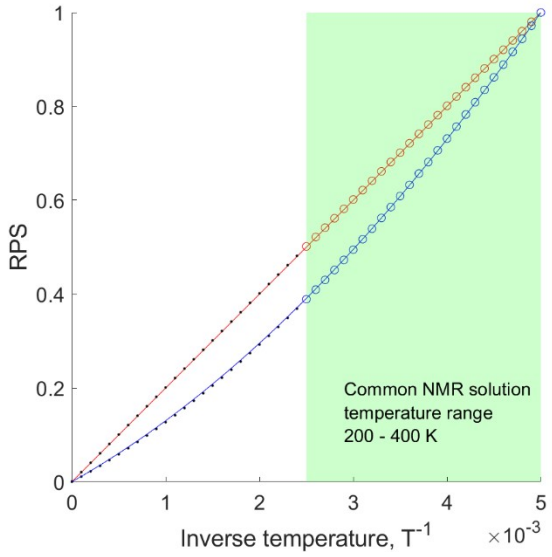

B) $g_x = g_y = 2.22$, $g_z = 2.86$, $D = -95$ cm^{-1}.[2]

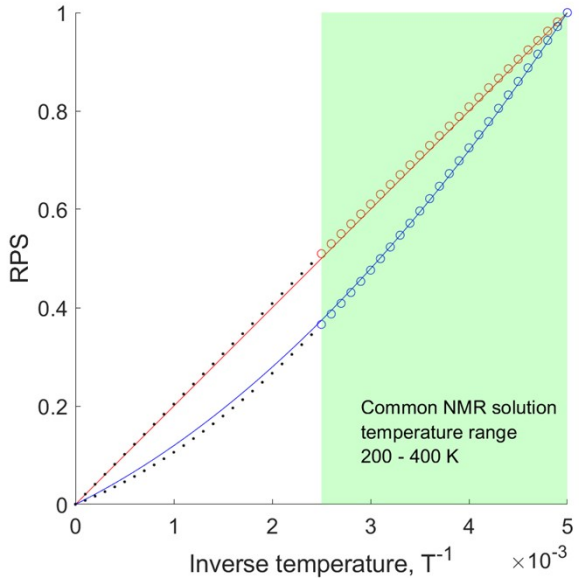

C) g = 2.06, L = 1, λ = –161 cm^{-1}, σ = 1.35, Δ = 663 cm^{-1}.[3]

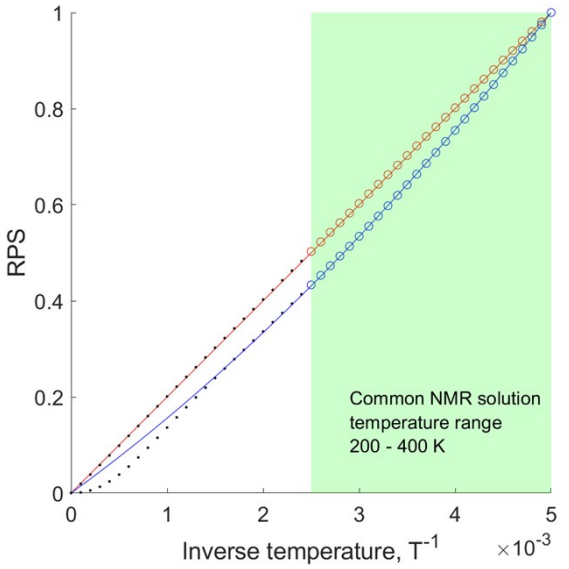

D) g = 2, L = 1, λ = –136 cm^{-1}, σ = 1.25, Δ = –502 cm^{-1}.[4]

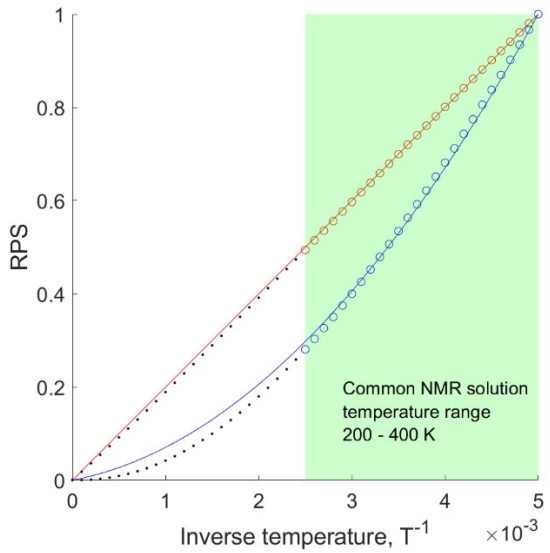

S.1.2. Fe(III), S = 1/2

A) $g_x = g_y = 2$, $g_z = 3$

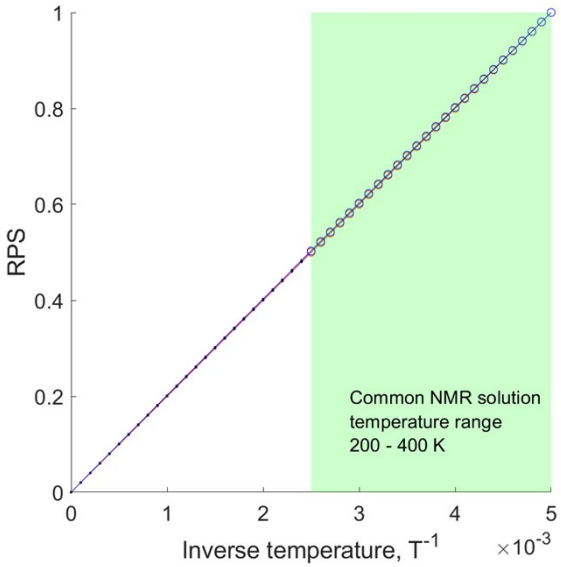

B) $g_x = g_y = g_z = 2$, L = 1, $\lambda = -460\ cm^{-1}$, $\sigma = 0.2$, $\Delta = -1000\ cm^{-1}$

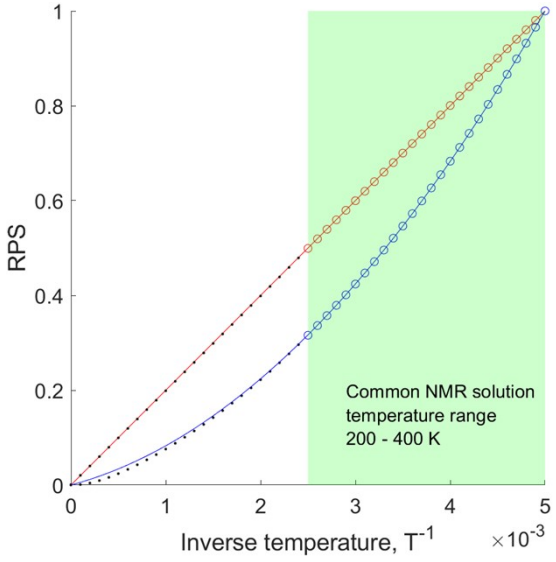

S.1.3. Fe(II), S = 2

A) $g_x = 2.02$, $g_y = 2.00$, $g_z = 2.08$, $D = -7.28$ cm^{-1}.[5]

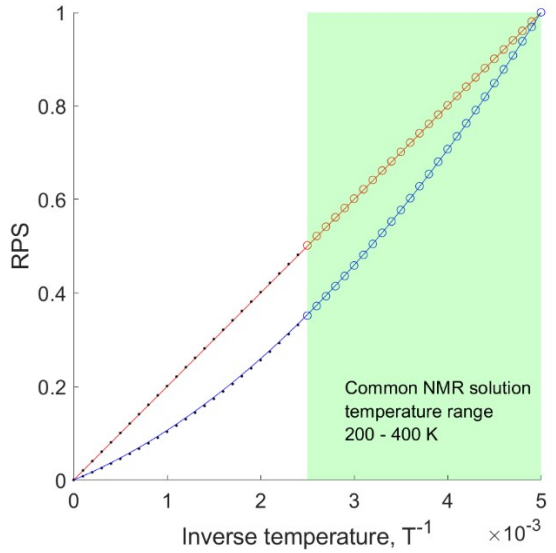

A) $g_x = g_y = 2.18$, $g_z = 2.023$, $D = +11.34$ cm^{-1}.[6]

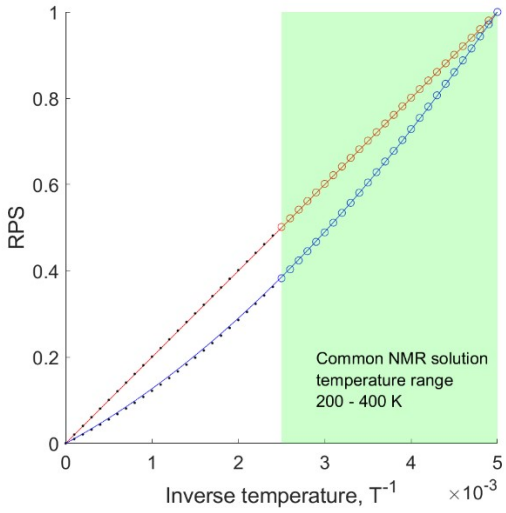
RPS
Inverse temperature, T-1
×10-3
Common NMR solution
temperature range
200 - 400 K

S.2. Detailed derivation of the RPS approach.

The following assumptions given by the equations 4a and 5a of the main text are used:

$$\delta_c(T) = aT^{-1} \quad (4a),$$

$$\delta_{pc}(T) = b_1T^{-1} + b_2T^{-2} \quad (5a).$$

Below is the proof of the equations 4b and 5b of the main text:

$$\Delta_c(T) = T_{min}T^{-1} \quad (4b),$$

$$\Delta_{pc}(T) = T_{min}T^{-1} + b \cdot \left(T^{-2} - T_{min}^{-1}T^{-1}\right) \quad (5b).$$

Reduced paramagnetic shift (RPS) for a contact or pseudocontact shift is equal to:

$$\Delta_c(T) = \frac{\delta_c(T)}{\delta_c(T_{min})} = \frac{aT^{-1}}{\delta_c(T_{min})} = a'T^{-1},$$

$$\Delta_{pc}(T) = \frac{\delta_{pc}(T)}{\delta_{pc}(T_{min})} = \frac{b_1T^{-1} + b_2T^{-2}}{\delta_{pc}(T_{min})} = b_1'T^{-1} + b_2'T^{-2}.$$

By the definition:

$$\Delta_c(T_{min}) = \Delta_{pc}(T_{min}) = 1.$$

The constant a' can be expressed as:

$$\Delta_c(T_{min}) = 1 = a'T_{min}^{-1},\ a' = T_{min}.$$

Using the above expression, the equation 4b becomes as follows:

$$\Delta_c(T) = T_{min}T^{-1}. \quad (4b).$$

The constant b_1' can be expressed as:

$$\Delta_{pc}(T_{min}) = 1 = b_1'T_{min}^{-1} + b_2'T_{min}^{-2},\ b_1' = T_{min} - b_2'T_{min}^{-1}.$$

Using the above expression, the equation 5b becomes as follows:

$$\Delta_{pc}(T) = \left(T_{min} - b_2'T_{min}^{-1}\right)T^{-1} + b_2'T^{-2} = T_{min}T^{-1} + b_2' \cdot \left(T^{-2} - T_{min}^{-1}T^{-1}\right).$$

By changing b_2' to b for simplicity:

$$\Delta_{pc}(T) = T_{min}T^{-1} + b \cdot \left(T^{-2} - T_{min}^{-1}T^{-1}\right).$$ (5b).

S.2.1. The case 1: the signs of δ^c and δ^{pc} are the same.

The absolute value of the pseudocontact shift is expressed as follows (eq. 7 of the main text):

$$\eta = \frac{\left|\delta_{pc}(T_{min})\right|}{\left|\delta_{pc}(T_{min})\right| + \left|\delta_c(T_{min})\right|} \quad (7).$$

The equation (7) takes the following form:

$$\eta = \frac{\delta_{pc}(T_{min})}{\delta_{pc}(T_{min}) + \delta_c(T_{min})} = \frac{\delta_{pc}(T_{min})}{\delta_{par}(T_{min})}. \quad (S1)$$

Then, the RPS temperature dependence of the total paramagnetic shift is equal to:

$$\Delta_{par}(T) = \frac{\delta_{par}(T)}{\delta_{par}(T_{min})} = \frac{\delta_{pc}(T)}{\delta_{par}(T_{min})} + \frac{\delta_c(T)}{\delta_{par}(T_{min})}. \quad (S2)$$

Given eq. (S1), the equation (S2) is transformed as follows:

$$\Delta_{par}(T) = \frac{\delta_{pc}(T)}{\delta_{pc}(T_{min})} \cdot \eta + \frac{\delta_c(T)}{\delta_c(T_{min})} \cdot (1-\eta) = \Delta_{pc}(T) \cdot \eta + \Delta_c(T) \cdot (1-\eta) \quad (S3).$$

The temperature dependences of $\Delta_c(T)$ and $\Delta_{pc}(T)$ are as follows (equations 4b and 5b):

$$\Delta_{par}(T) = \eta \cdot \left[T_{min}T^{-1} + b \cdot \left(T^{-2} - T_{min}^{-1}T^{-1}\right)\right] + (1-\eta) \cdot \left[T_{min}T^{-1}\right] =$$

$$= \left(T_{min} - \frac{\eta b}{T_{min}}\right) \cdot T^{-1} + \eta b \cdot T^{-2} \quad (S4).$$

The RPS temperature dependence of the total paramagnetic shift is considered as a quadratic dependence, as follows from the combination of the equations S3, 4b and 5b:

$$\Delta_{par}(T) = A \cdot T^{-1} + B \cdot T^{-2} \quad (S5).$$

By the comparison of (S4) and (S5), the expression for the absolute value of the pseudocontact shift becomes:

$$\eta = \frac{T_{min} \cdot (T_{min} - A)}{b} = \frac{B}{b}. \quad (S6)$$

Given the expression for the pseudocontact shift (3), the total paramagnetic shift at the lowest temperature is equal to:

$$\delta_{par}(T_{min}) = \frac{\delta_{pc}(T_{min})}{\eta} = \frac{(3cos^2\theta - 1) \cdot \Delta\chi(T_{min}) \cdot b}{12\pi r^3 \cdot B}. \quad \text{(S7)}$$

Finally, the expression for the total paramagnetic shift at any temperature is:

$$\delta_{par}(T) = \Delta_{par}(T) \cdot \delta_{par}(T_{min}) = \left(A \cdot T^{-1} + B \cdot T^{-2}\right) \cdot \frac{(3cos^2\theta - 1) \cdot \Delta\chi(T_{min}) \cdot b}{12\pi r^3 \cdot B}. \quad \text{(S8)}$$

S.2.1. The case 2: signs of δ^c and δ^{pc} are opposite.

The equation (7) takes the following form:

$$\eta = \frac{\delta_{pc}(T_{min})}{\delta_{pc}(T_{min}) - \delta_c(T_{min})} \quad \text{(S9)}$$

Therefore, the total paramagnetic shift at the lowest temperature can be expressed by two ways:

$$\delta_{par}(T_{min}) = \frac{\delta_{pc}(T_{min})}{\eta} \cdot (2\eta - 1) = -\frac{\delta_c(T_{min})}{1 - \eta} \cdot (2\eta - 1). \quad \text{(S10)}$$

Given (S2) and (S10), the expression for the total paramagnetic shift at any temperature becomes:

$$\Delta_{par}(T) = \frac{\delta_{pc}(T)}{\delta_{par}(T_{min})} + \frac{\delta_c(T)}{\delta_{par}(T_{min})} = \frac{\delta_{pc}(T) \cdot \eta}{\delta_{pc}(T_{min}) \cdot (2\eta - 1)} - \frac{\delta_c(T) \cdot (1 - \eta)}{\delta_c(T_{min}) \cdot (2\eta - 1)} =$$

$$= \Delta_{pc}(T)\frac{\eta}{(2\eta - 1)} - \Delta_c(T)\frac{(1 - \eta)}{(2\eta - 1)}. \quad \text{(S11)}$$

The temperature dependences of $\Delta_c(T)$ and $\Delta_{pc}(T)$ are as follows (equations 4b and 5b):

$$\Delta_{par}(T) = \left(T_{min} - \frac{\eta b}{T_{min}(2\eta - 1)}\right) \cdot T^{-1} + \frac{\eta b}{2\eta - 1} \cdot T^{-2}. \quad \text{(S12).}$$

By the comparison of (S5) and (S12), the expressions for the absolute value of the pseudocontact shift becomes:

$$\eta = \frac{A - T_{min}}{2\left(A - T_{min}\right) + \frac{b}{T_{min}}} = \frac{B}{2B - b} \quad . \tag{S13}$$

Given the expression for the pseudocontact shift (3) and the equation (S10), the total paramagnetic shift at the lowest temperature is equal to:

$$\delta_{par}(T_{min}) = \delta_{pc}(T_{min})\left(2 - \frac{1}{\eta}\right) = \frac{\left(3cos^2\theta - 1\right) \cdot \Delta\chi(T_{min})}{12\pi r^3} \cdot \left(2 - \frac{1}{\eta}\right). \tag{S14}$$

Finally, the expression for the total paramagnetic shift at any temperature is the same as in the first case:

$$\delta_{par}(T) = \Delta_{par}(T) \cdot \delta_{par}(T_{min}) = \left(A \cdot T^{-1} + B \cdot T^{-2}\right) \cdot \frac{\left(3cos^2\theta - 1\right) \cdot \Delta\chi(T_{min}) \cdot b}{12\pi r^3 \cdot B} \quad . \tag{S15}$$

S.3 Correlation between convexity/concavity of an RPS temperature dependence and the signs of total paramagnetic shift (δ^{par}) and its pseudocontact component (δ^{pc}).

Hypothesis: If the RPS temperature dependence is concave, then the signs of the total paramagnetic shift (δ^{par}) and its pseudocontact component (δ^{pc}) are the same, and *vice versa*, if it is convex, then the signs of these shifts are opposite.

Proof: The convexity/concavity of the RPS temperature dependence is defined by the second derivative, which is as follows (given S4 and S12):

$$\frac{\partial^2 \Delta_{par}(T)}{\partial\left(T^{-1}\right)^2} = 2\eta b \qquad \text{(S16)}$$

for the first case described in the **S.2** (signs of δ^c and δ^{pc} are the same) and

$$\frac{\partial^2 \Delta_{par}(T)}{\partial\left(T^{-1}\right)^2} = \frac{2\eta b}{2\eta - 1} \qquad \text{(S17)}$$

for the second case described in the **S.2** (signs of δ^c and δ^{pc} are opposite).

As a rule, signs of D and Δg ($g_{||} - g_{\perp}$) are opposite for d^5-d^9 transition ions due to their negative spin-orbit coupling [F.E. Mabbs and D. Collison Electron Paramagnetic Resonance of d Transition Metal Compounds-Elsevier Science (1992), ch. 10]. The value of D is negative and $g_{||} > g_{\perp}$ in a so-called 'easy-axis' case. Conversely, an 'easy plane' case corresponds to the positive D and $g_{||} < g_{\perp}$. In both cases, the temperature dependence of the absolute value of the pseudocontact shift has a concave shape (i.e., $b \geq 0$), as can be shown by applying simplified expressions for the pseudocontact shift [J. Chem. Phys. 142, 054108 (2015)] or direct calculations through spin-Hamiltonian from section **S.1**.

In the first case, the RPS temperature dependence is always concave ($\frac{\partial^2 \Delta_{par}(T)}{\partial\left(T^{-1}\right)^2} > 0$), and the signs of the total paramagnetic shift (δ^{par}) and its pseudocontact component (δ^{pc}) are the same by the definition. Therefore, the hypothesis is proved for this case.

For the second case (signs of δ^c and δ^{pc} are opposite), the RPS temperature dependence is concave ($\frac{\partial^2 \Delta_{par}(T)}{\partial\left(T^{-1}\right)^2} > 0$) at $\eta > 0.5$, so that the pseudocontact shift defines the sign of the total paramagnetic shift, as it is larger (by the absolute value) than the contact shift.

S.4. DFT-based approach for the analysis of NMR spectra

Quantum chemical calculations of the studied complexes were performed using ORCA package, v.4.2.[7];[8] X-ray diffraction geometries [2, 9-11] were chosen as a starting point for geometry optimization with the B3LYP functional, [12-14] [15] the scalar relativistic zero-order regular approximation (ZORA),[16] Grimme's DFT-D3 dispersion correction [17] and the scalar relativistically recontracted (SARC) [18] version of the def2-TZVP basis set.[19] To speed up the calculations, the RIJCOSX approximation[20] with a def2/J fitting basis set[21] was used. In all cases, extra tight thresholds for forces and displacements were used.

The resulting geometries of the complexes were used to compute g-tensor and isotropic values of hyperfine interaction tensors A_{iso} for each nucleus at the same level of theory (PBE0/def2-TZVP). Isotropic paramagnetic (contact) contribution δ_c to the chemical shifts in the NMR spectra was evaluated through the following equation:[22]

$$\delta^c = \frac{S(S+1)\mu_B}{3kTg_N\mu_N} \cdot \bar{g} \cdot A_{iso},$$

($\bar{g}$ – calculated rotationally averaged electronic g-value, g_N – nuclear g-value, μ_B – Bohr magneton, μ_N – nuclear magneton, kT – thermal energy).

The value for the anisotropy of the magnetic susceptibility $\Delta\chi$ was estimated by fitting the observed chemical shifts in the NMR spectra to those estimated by the following equation:

$$\delta_{OBS} = \delta^{DIA} + \delta^c + \frac{1}{12\pi r^3}\left[\Delta\chi\left(3cos^2\theta - 1\right)\right],$$

In this expression, $\Delta\chi$ stands for the axial anisotropy of the magnetic susceptibility tensor (χ–tensor). The polar coordinates of the nuclei *r* and θ were taken from the optimized geometries of the complexes (as explained above), and the diamagnetic contribution (δ^{DIA}) was taken as the chemical shift from the closest diamagnetic analogue, such as a free ligand or an isostructural complex with a diamagnetic metal ion.

S.5. NMR spectra

^{1}H NMR spectra were acquired via Bruker Avance 300 NMR spectrometer (300.15 MHz). Chemical shift values were referenced by residual signal of a solvent (CD_2Cl_2 – 5.32 ppm; CD_3CN – 1.94 ppm), which allowed to avoid susceptibility shifts. Sample temperature was calibrated using the standard Bruker reference (4% methanol in methanol-d4) in temperature range 190–300 K by the following equations:

190–230 K: $T = (3.72 - \Delta)/0.007143$,

230–270 K: $T = (3.92 - \Delta)/0.008$,

270–300 K: $T = (4.109 - \Delta)/0.008708$

with Δ is the shift difference (ppm) between the CH_3 and OH peaks.

Higher temperatures up to 345 K were calibrated using 100% ethylene glycol:

$T = (4.637 - \Delta)/0.009967$

with Δ is the shift difference (ppm) between the CH_2 and OH peaks.

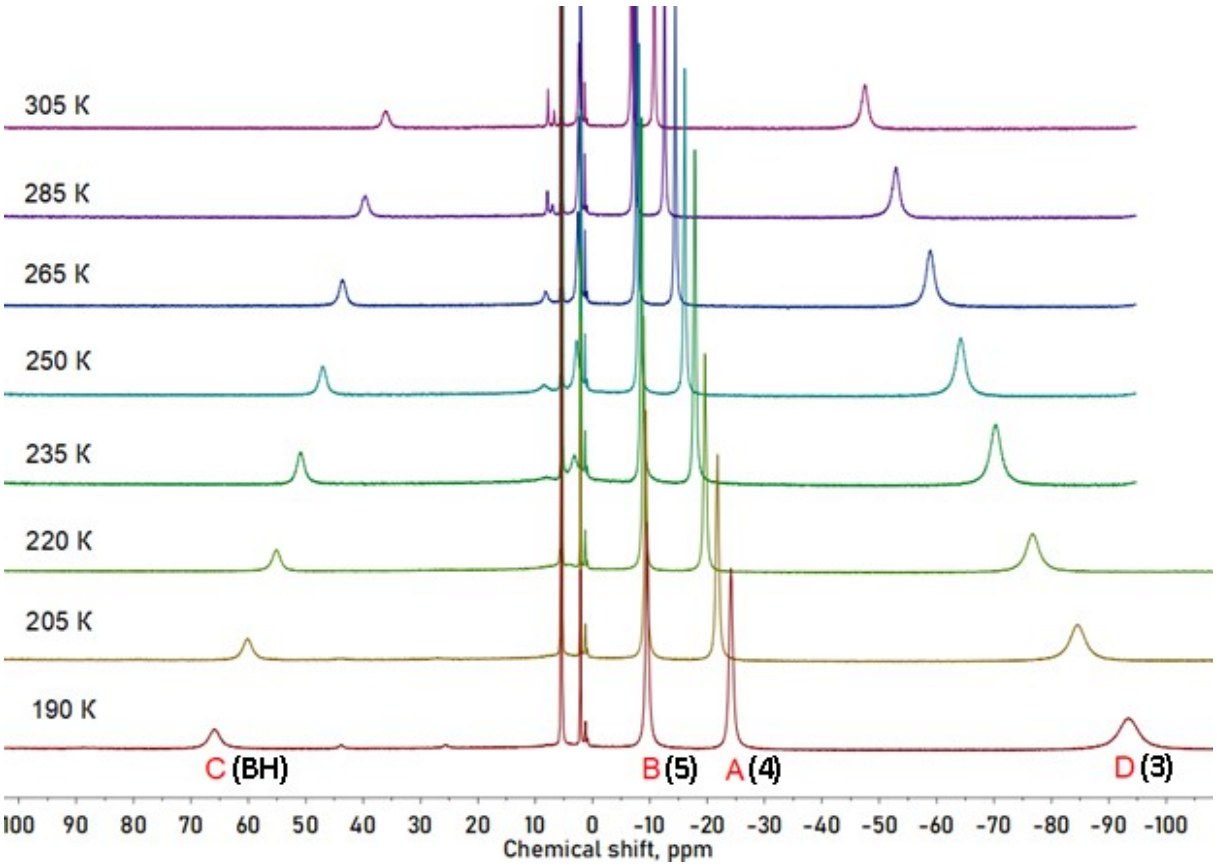

Figure S1. Variable-temperature ^{1}H NMR spectra of complex **1** in CD_2Cl_2 solution (300 MHz). Signals are assigned to nuclei as it is shown on the Scheme 1.

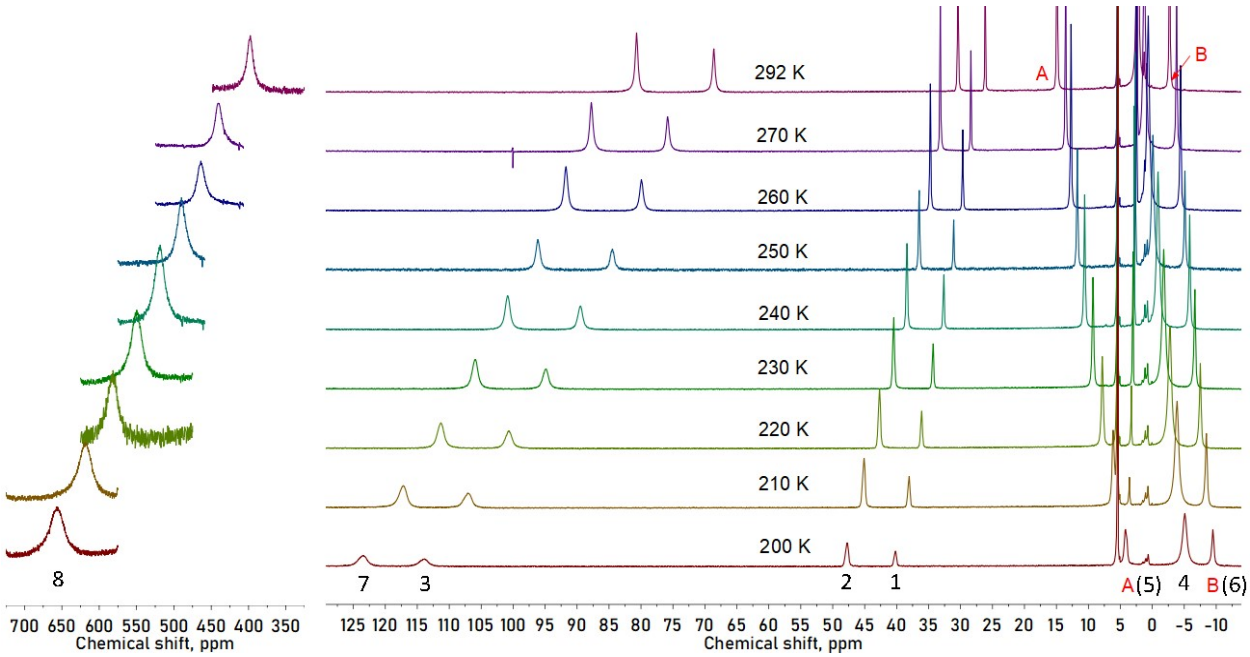

Figure S2. Variable-temperature ^{1}H NMR spectra of complex **2** in CD_2Cl_2 solution (300 MHz). Signals are assigned to nuclei as it is shown on the Scheme 1.

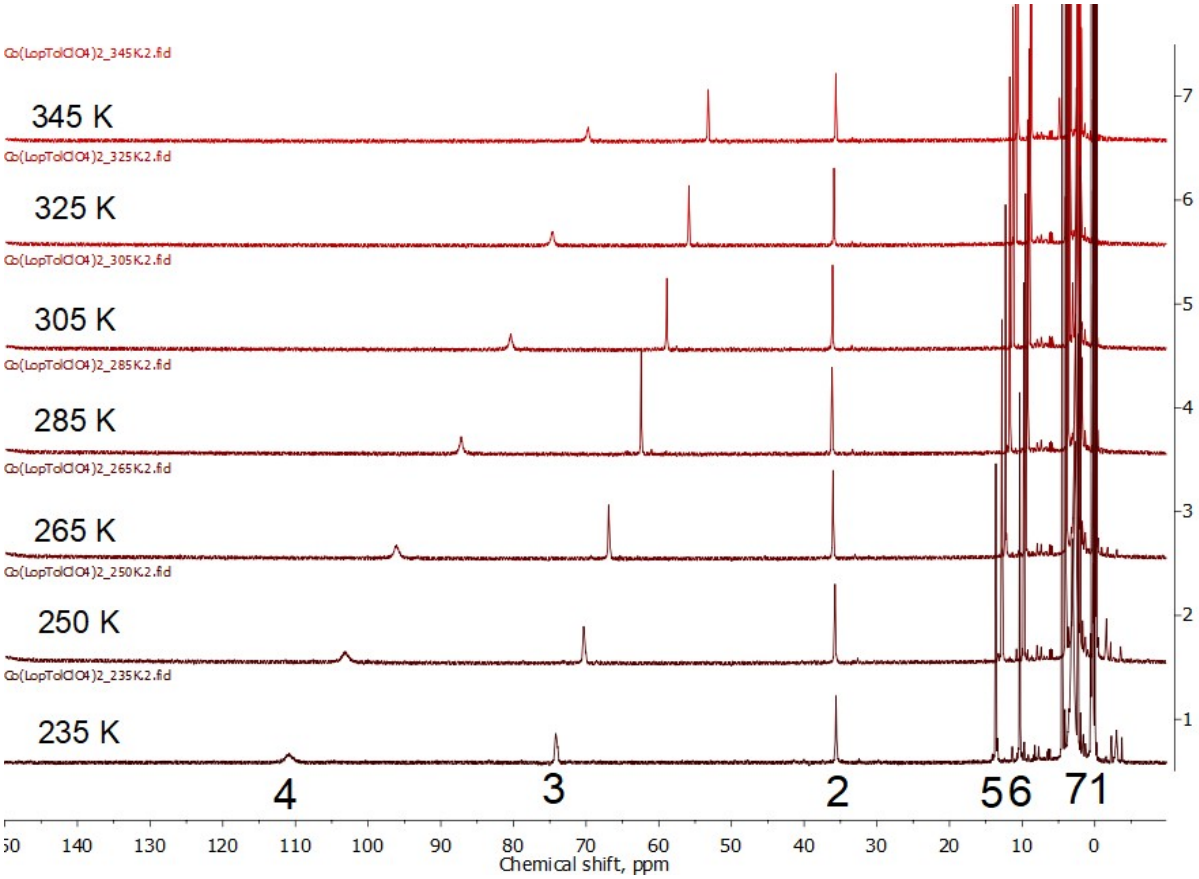

Figure S3. Variable-temperature ^{1}H NMR spectra of complex **3** in CD_3CN solution (300 MHz). Signals are assigned to nuclei as it is shown on the Scheme 1.

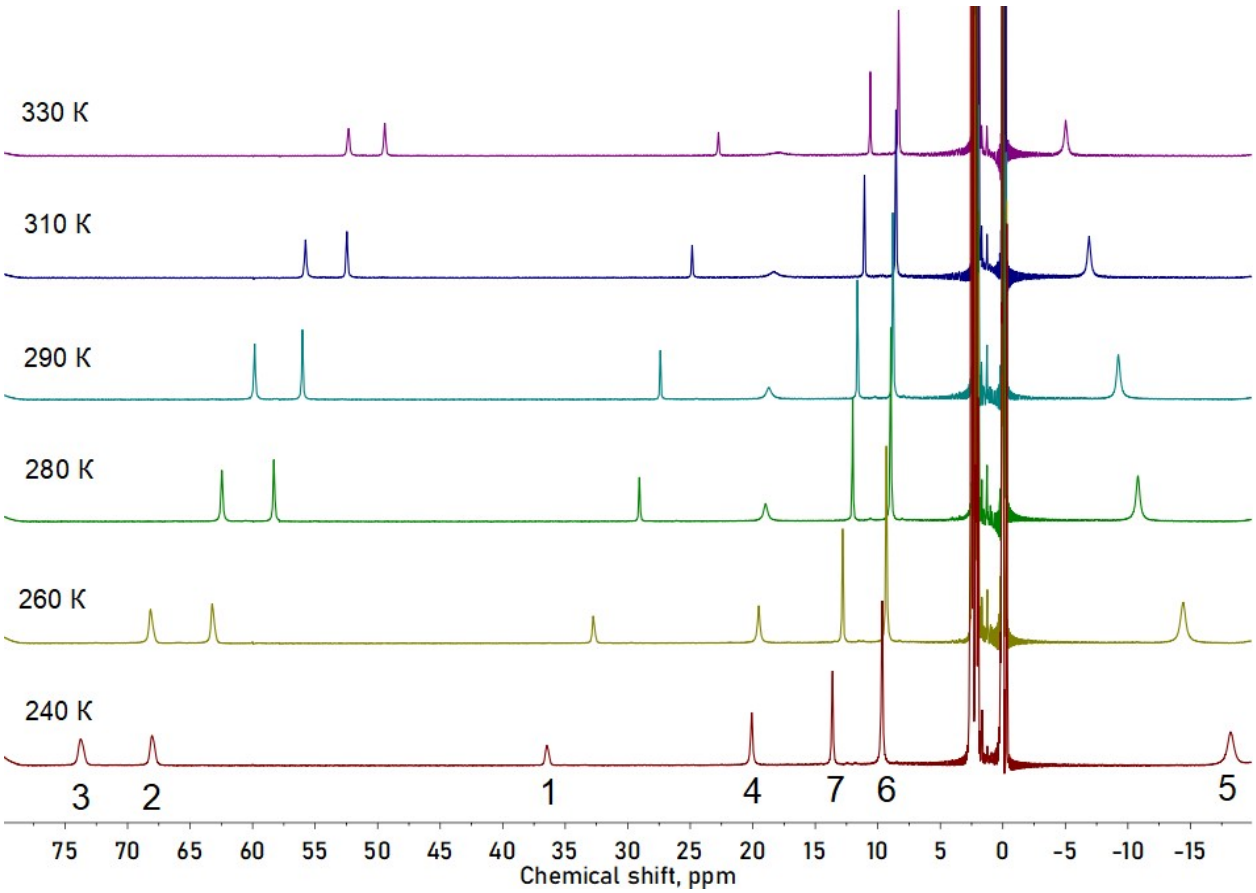

Figure S4. Variable-temperature ^{1}H NMR spectra of complex **4** in CD_3CN solution (300 MHz). Signals are assigned to nuclei as it is shown on the Scheme 1.

S.6. Synthesis

Complex **1**. Potassium tris(3,5-dimethyl-1-pyrazolyl)borate (0.4 mmol, 100 mg) and $FeCl_3 \cdot 6H_2O$ (0.2 mmol, 54 mg) were added to methanol (5 mL). In 30 min, $NaBF_4$ (0.21 mmol, 23 mg) was added to the resulting red solution, which was then stirred for 30 min. The solution was filtered and evaporated to dryness. Crude product was recrystallized by the liquid diffusion of diethyl ether into a methanol solution to produce red crystals. Yield: 99 mg (87%). Elemental analysis: calcd (%) for $C_{18}H_{20}B_2CoN_{12}$ (**2**): C (38.01), N (29.56), H (3.54); found C (38.15), N (29.43), H (3.65). ^{1}H NMR (300 MHz, 305 K, CD_2Cl_2): –47.6 (s, 2H, 3), –10.83 (s, 2H, 4), –6.85 (s, 2H, 5), 35.9 (s, 2H, BH).

Complexes **2**–**4** were synthesized as reported earlier.[2, 10, 11]

Complex **2**: ^{1}H NMR (300 MHz, 298 K, CD_2Cl_2): δ, ppm = – 2.50 (s, 3H, 3-Py), 2.42 (s, 9H, CH_3), 15.12 (s, 3H, 4-Py), 25.71 (s, 1H, *p*-Ph), 29.93 (s, 2H, *m*-Ph), 67.86 (s, 2H, *o*-Ph), 80.12 (s, 3H, 5-Py), 396.17 (br. s, 3H, 6-Py).

Complex **3**: ^{1}H NMR (300 MHz, 298 K, CD_3CN): δ(ppm) = 2.04 (*p*-Py, s, 2H), 3.54 (Me, s, 12H), 9.09(*o*-Ph(Me), d, $^3J_{HH}$ = 5.8 Hz, 8H), 11.42 (*m*-Ph(Me), d, $^3J_{HH}$ = 5.8 Hz, 8H), 36.07 (*m*-Py, br. s, 4H), 60.78 (Pr, br. s, 4H), 84.06 (NH, br. s, 4H).

Complex **4**: ^{1}H NMR (300 MHz, 290 K, CD_3CN,): δ = 59.74 (s, 4H, 3), 56.04 (s, 4H, 2), 27.44 (s, 2H, 1), 18.71 (s, 4H, 4), 11.63 (s, 4H, 7), 8.80 (s, 8H, 6), −9.25 (s, 8H, 5).

S.7. References

1. Zadrozny, J. M.; Liu, J.; Piro, N. A.; Chang, C. J.; Hill, S.; Long, J. R. Slow magnetic relaxation in a pseudotetrahedral cobalt (II) complex with easy-plane anisotropy. *Chemical Communications* **2012,** 48 (33), 3927-3929.

2. Pavlov, A. A.; Savkina, S. A.; Belov, A. S.; Nelyubina, Y. V.; Efimov, N. N.; Voloshin, Y. Z.; Novikov, V. V. Trigonal prismatic tris-pyridineoximate transition metal complexes: A cobalt (II) compound with high magnetic anisotropy. *Inorganic chemistry* **2017,** 56 (12), 6943-6951.

3. Palacios, M. A.; Nehrkorn, J.; Suturina, E. A.; Ruiz, E.; Gómez-Coca, S.; Holldack, K.; Schnegg, A.; Krzystek, J.; Moreno, J. M.; Colacio, E. Analysis of magnetic anisotropy and the role of magnetic dilution in triggering single-molecule magnet (SMM) behavior in a family of CoIIYIII dinuclear complexes with easy-plane anisotropy. *Chemistry–A European Journal* **2017,** 23 (48), 11649-11661.

4. Wu, Y.; Tian, D.; Ferrando-Soria, J.; Cano, J.; Yin, L.; Ouyang, Z.; Wang, Z.; Luo, S.; Liu, X.; Pardo, E. Modulation of the magnetic anisotropy of octahedral cobalt (II) single-ion magnets

by fine-tuning the axial coordination microenvironment. *Inorganic Chemistry Frontiers* **2019,** 6 (3), 848-856.

5. Novitchi, G. n.; Jiang, S.; Shova, S.; Rida, F.; Hlavička, I.; Orlita, M.; Wernsdorfer, W.; Hamze, R.; Martins, C.; Suaud, N. From positive to negative zero-field splitting in a series of strongly magnetically anisotropic mononuclear metal complexes. *Inorganic chemistry* **2017,** 56 (24), 14809-14822.

6. Telser, J.; van Slageren, J.; Vongtragool, S.; Dressel, M.; Reiff, W. M.; Zvyagin, S.; Ozarowski, A.; Krzystek, J. High-frequency/high-field EPR spectroscopy of the high-spin ferrous ion in hexaaqua complexes. *Magnetic Resonance in Chemistry* **2005,** 43 (S1), S130-S139.

7. Neese, F. The ORCA program system. *Wiley Interdisciplinary Reviews: Computational Molecular Science* **2012,** 2 (1), 73-78.

8. Neese, F. Software update: the ORCA program system, version 4.0. *Wiley Interdisciplinary Reviews: Computational Molecular Science* **2018,** 8 (1), e1327.

9. Cho, S.-H.; Whang, D.-M.; Kim, K.-M. Synthesis and Structure of Bis [hydrotris (1-pyrazolyl) borato] iron (III) Nitrate. *Bulletin of the Korean Chemical Society* **1991,** 12 (1), 107-109.

10. Pavlov, A. A.; Aleshin, D. Y.; Nikovskiy, I. A.; Polezhaev, A. V.; Efimov, N. N.; Korlyukov, A. A.; Novikov, V. V.; Nelyubina, Y. V. New Spin-Crossover Complexes of Substituted 2, 6-Bis (pyrazol-3-yl) pyridines. *European Journal of Inorganic Chemistry* **2019,** 2019 (23), 2819-2829.

11. Nelyubina, Y.; Polezhaev, A.; Pavlov, A.; Aleshin, D.; Savkina, S.; Efimov, N.; Aliev, T.; Novikov, V. Intramolecular Spin State Locking in Iron (II) 2, 6-Di (pyrazol-3-yl) pyridine Complexes by Phenyl Groups: An Experimental Study. *Magnetochemistry* **2018,** 4 (4), 46.

12. Antony, J.; Grimme, S. Density functional theory including dispersion corrections for intermolecular interactions in a large benchmark set of biologically relevant molecules. *Physical Chemistry Chemical Physics* **2006,** 8 (45), 5287-5293.

13. Lee, C.; Yang, W.; Parr, R. G. Development of the Colle-Salvetti correlation-energy formula into a functional of the electron density. *Physical review B* **1988,** 37 (2), 785.

14. Vosko, S. H.; Wilk, L.; Nusair, M. Accurate spin-dependent electron liquid correlation energies for local spin density calculations: a critical analysis. *Canadian Journal of physics* **1980,** 58 (8), 1200-1211.

15. Stephens, P. J.; Devlin, F. J.; Chabalowski, C. F.; Frisch, M. J. Ab initio calculation of vibrational absorption and circular dichroism spectra using density functional force fields. *The Journal of physical chemistry* **1994,** 98 (45), 11623-11627.

16. van Wüllen, C. Molecular density functional calculations in the regular relativistic approximation: Method, application to coinage metal diatomics, hydrides, fluorides and chlorides, and comparison with first-order relativistic calculations. *The Journal of chemical physics* **1998,** 109 (2), 392-399.

17. Grimme, S.; Antony, J.; Ehrlich, S.; Krieg, H. A consistent and accurate ab initio parametrization of density functional dispersion correction (DFT-D) for the 94 elements H-Pu. *The Journal of chemical physics* **2010,** 132 (15), 154104.

18. Pantazis, D. A.; Chen, X.-Y.; Landis, C. R.; Neese, F. All-electron scalar relativistic basis sets for third-row transition metal atoms. *Journal of chemical theory and computation* **2008,** 4 (6), 908-919.

19. Weigend, F.; Ahlrichs, R. Balanced basis sets of split valence, triple zeta valence and quadruple zeta valence quality for H to Rn: Design and assessment of accuracy. *Physical Chemistry Chemical Physics* **2005,** 7 (18), 3297-3305.

20. Neese, F. An improvement of the resolution of the identity approximation for the formation of the Coulomb matrix. *Journal of computational chemistry* **2003,** 24 (14), 1740-1747.

21. Weigend, F. Accurate Coulomb-fitting basis sets for H to Rn. *Physical chemistry chemical physics* **2006,** 8 (9), 1057-1065.

22. Kaupp, M.; Buhl, M.; Malkin, V. G. *Calculation of NMR and EPR Parameters*. Wiley Online Library: 2004.